Author/s:
Wong, VHY;Zhao, D;Bui, BV;Millar, CJ;Nguyen, CTO

Title:
Increased episcleral venous pressure in a mouse model of circumlimbal suture induced ocular hypertension

Date:
2021-01-01

Citation:
Wong, V. H. Y., Zhao, D., Bui, B. V., Millar, C. J. & Nguyen, C. T. O. (2021). Increased episcleral venous pressure in a mouse model of circumlimbal suture induced ocular hypertension. Experimental Eye Research, 202, https://doi.org/10.1016/j.exer.2020.108348.

Persistent Link:
https://hdl.handle.net/11343/301991

Experimental Eye Research xxx (xxxx) xxx

Contents lists available at ScienceDirect

Experimental Eye Research

journal homepage: www.elsevier.com/locate/yexer

# Increased episcleral venous pressure in a mouse model of circumlimbal suture induced ocular hypertension☆

Vickie H.Y. Wong [a], Da Zhao [a], Bang V. Bui [a], Cameron J. Millar [b], Christine T.O. Nguyen [a,*]

[a] Department of Optometry and Vision Sciences, University of Melbourne, Parkville, Victoria, Australia
[b] North Texas Eye Research Institute, Department of Pharmacology and Neuroscience, University of North Texas Health Science Center, Fort Worth, Texas, USA

ARTICLE INFO

*Keywords:*
Mouse
IOP
Aqueous dynamics

ABSTRACT

*Purpose:* To investigate changes in aqueous humor dynamics during intraocular pressure (IOP) elevation induced by circumlimbal suture in mice.
*Methods:* Ocular hypertension (OHT) was induced by applying a circumlimbal suture behind the limbus in male adult C57BL6/J mice. In the OHT group, the suture was left in place for an average of 8 weeks (n = 10, OHT group). In the sham control group the suture was cut at 2 days (n = 9, sham group) and in the naïve control group (n = 5) no suture was implanted. IOP was measured at baseline across 3 days, 1 h post-suture implantation, and at the chronic endpoint. Anterior segments were assessed using optical coherence tomography (OCT). Episcleral venous pressure (EVP), total outflow facility (C), uveoscleral outflow (Fu) and aqueous humor flow rate (Fin) were determined using a constant-flow infusion model.
*Results:* All aqueous dynamic and chronic IOP outcome measures showed no difference between sham and naïve controls ($p > 0.05$) and thus these groups were combined into a single control group. IOP was elevated in OHT group compared with controls ($p < 0.01$). Chronic suture implantation did not change pupil size, anterior chamber depth or iridocorneal angles ($p > 0.05$). EVP was significantly higher in OHT eyes compared to control eyes ($p < 0.01$). There was no statistical difference in C, Fu and Fin between groups ($p > 0.05$). A significant linear correlation was found between IOP and EVP ($R^2 = 0.35$, $p = 0.001$).
*Conclusions:* Circumlimbal suture implantation in mouse eyes results in chronic IOP elevation without angle closure. Chronic IOP elevation is likely to reflect higher EVP.

## 1. Introduction

Glaucoma is a multifaceted neurodegenerative condition characterised by progressive retinal ganglion cell loss and optic nerve degeneration. Elevated intraocular pressure (IOP) is the most well-defined and only modifiable risk factor in glaucoma (Cook and Foster, 2012; Kass et al., 2002; Zhan et al., 2002). Glaucoma is characterised by retinal ganglion cell dysfunction and retinal nerve fibre layer thinning as has been documented in both laboratory and clinic studies (Fortune et al., 2004; Pollet-Villard et al., 2014; Saleh et al., 2007; Viswanathan et al., 2001). Rodent models are commonly used in glaucoma research as they are inexpensive and suitable for longitudinal assessment. Mice models also have distinct advantages in terms of the availability of genetic tools to probe our understanding of disease pathogenesis. Mice show IOP levels similar to those seen in humans (Johnson and Tomarev, 2010; Martinez-Aguila et al., 2016), and have similar aqueous humor dynamics relative to human eyes (Johnson and Tomarev, 2010; Pang and Clark, 2007). Because of these similarities and advantages, mice are increasingly used by glaucoma researchers, notwithstanding differences in optic nerve structure (Fischer et al., 2009; Jeon et al., 1998).

There are a variety of rodent glaucoma models, each with distinct advantages and disadvantages. The circumlimbal suture model (He et al., 2018; Lee et al., 2019; Liu et al., 2017a, 2017b; Zhao et al., 2017, 2019) employed in this study produces sustained mild and stable IOP elevation, preferential loss of retinal ganglion cells, clear optics to facilitate in vivo imaging and ease of IOP normalization (suture removal) without potential confounds associated with pharmacological intervention (He et al., 2018; Liu et al., 2017a; Zhao et al., 2017, 2019). However, the mechanism of IOP elevation in the circumlimbal approach has not yet been examined. This knowledge would better inform the use

☆ Vickie H.Y. Wong and Da Zhao contributed equally to the work and should therefore be regarded as equivalent first authors.

* Corresponding author. Christine Nguyen Department of Optometry and Vision Sciences, The University of Melbourne, Parkville, 3010, Victoria, Australia.
*E-mail address:* christine.nguyen@unimelb.edu.au (C.T.O. Nguyen).

https://doi.org/10.1016/j.exer.2020.108348
Received 2 May 2020; Received in revised form 29 October 2020; Accepted 3 November 2020
Available online 6 November 2020

of this model for glaucoma research.

The level of IOP in the eye is determined by a balance between a range of factors. Aqueous humor (AH) is produced by the ciliary body and drains out of the eye through the 'conventional route' (trabecular meshwork) or 'unconventional' route (uveoscleral and uveovortex pathways) (Johnson et al., 2017). The trabecular meshwork pathway (otherwise known as the pressure sensitive pathway) involves aqueous draining through the trabecular meshwork into the Schlemm's canal which feeds into the episcleral venous network (Gong et al., 1996; Johnson et al., 2002; Tamm, 2009). The majority of aqueous outflow occurs through this pathway, but a certain proportion also flows out the uveoscleral pathway. The uveoscleral route (or pressure-insensitive pathway) involves AH drainage between the iris and ciliary muscle bundles which is then absorbed by orbital blood vessels surrounding these muscles. A fraction of this AH is taken up by the choroidal vessels via osmosis and drained into the vortex veins (uveovortex outflow). The pressure gradient that exists between the higher-pressure anterior chamber (IOP) to the lower pressure episcleral veins (EVP) facilitates aqueous outflow. The relationship between IOP and AH dynamic parameters can be described by a modified Goldmann equation (Becker and Neufeld, 2002; Brubaker, 2004; Goldmann, 1951; Mermoud et al., 1996; Millar et al., 2011) where *Fin* is the AH production rate, *Fu* is the uveoscleral outflow rate, *C* is the outflow facility and *EVP* is the episcleral venous pressure (Equation (1)).

$$IOP = \left[\frac{(Fin\cdot - Fu)}{C}\right] + EVP \quad [1]$$

The mechanism of IOP elevation varies depending on the type of glaucoma. In angle closure glaucoma, aqueous outflow is compromised through physical obstruction of the drainage pathways. In chronic primary open angle glaucoma, it has been shown that increased outflow resistance in the trabecular pathway contributes to elevated IOP (Allingham et al., 1996; Alvarado and Murphy, 1992; Becker and Hahn, 1964; Jackson et al., 2006; Tamm and Fuchshofer, 2007) and some studies indicate a role for elevated EVP (Greenfield, 2000; Greslechner and Oberacher-Velten, 2019; Jorgensen and Guthoff, 1988; Selbach et al., 2005), however the exact mechanisms still remain unclear. In terms of animal studies, current rodent glaucoma models target the trabecular meshwork or episcleral vein outflow routes to elevate eye pressure. For example, the microbead injection model (Chen et al., 2011; Smedowski et al., 2014) and laser photocoagulation model (Kwong et al., 2011; Levkovitch-Verbin et al., 2002) aim to clog and scar the trabecular meshwork which should lower outflow facility (*C*), and other models like the episcleral vein cauterization (Anders et al., 2017; Liu et al., 2017b; Ruiz-Ederra and Verkman, 2006; Shareef et al., 1995) and ligation models (Dey et al., 2018; Yu et al., 2006) scar and tie off episcleral veins, thus an elevation of EVP would be expected. The circumlimbal suture model involves attaching and tightening a thin thread behind the limbus to apply inward compression of the globe and surrounding episcleral veins (He et al., 2018). However, the exact mechanism by which this model induces chronic IOP elevation has not yet been examined.

## 2. Materials and methods

### 2.1. Animals

In total 24 adult male C57BL/6J mice aged 3 months old (Animal Resource Centre, Caning Vale, WA, Australia) were used in this study. All procedures were conducted in accordance with the National Health and Medical Research Council of Australia guide for the use of animals in research and conformed with the ARVO Statement for the Use of Animals in Ophthalmic and Vision Research. Animal ethics was approved by the Howard Florey Animal Ethics Committee (ethics number: 13-068-UM). Mice were housed in the Melbourne Brain Centre (Parkville, VIC, Australia) with free access to water and chow (Barastoc, Melbourne, VIC, Australia). Room temperature was kept at 21 °C, with animals exposed to a 12-h light/dark cycle (lights on at 7 am/off at 7pm, < 50 lux inside the cage).

Animals were allocated into three groups: an ocular hypertension group (OHT, n = 10) and a control group which included a suture cut sub-cohort (sham, n = 9) and an age-matched naïve sub-cohort (naïve, n = 5). All animals were handled daily for one week prior to the experiment for acclimation. One eye of each mouse was randomly chosen as the IOP-treated eye, and end-point assessment was conducted during the chronic phase of IOP elevation (He et al., 2018; Liu et al., 2015; Zhao et al., 2017, 2019), between 6 and 10 weeks (average 8 weeks) after circumlimbal suture placement.

For suture implantation, to achieve stable sedation, conscious mice were induced with a relatively higher isoflurane rate (IsoFlo®, 3.5% isoflurane with oxygen at a flow rate of 3 L/min), and then switched to a lower rate (1.5% isoflurane with oxygen at a flow rate of 1.5 L/min) to maintain sedation via the RotaFlush™ anesthetic system (Medical Developments International Ltd, Springvale, VIC, Australia). During endpoint examinations, animals were anesthetized by intraperitoneal injection of a ketamine and xylazine mixture (80 and 10 mg/kg respectively, Troy Laboratory, Glendenning, NSW, Australia). Animals were given a top-up dose (half initial dose) every 45 min. A drop of local anesthetic (0.5% proxymetacaine, Alcaine, Alcon Laboratories, Frenchs Forest, NSW, Australia) and mydriatic (1% tropicamide, Mydriacyl, Alcon Laboratories) were given to obtain corneal anesthesia and pupil dilation, respectively. During anesthesia, body temperature (~37 °C) was maintained by using an electrical heat pad. A ketamine over-dose (>150 mg/kg intraperitoneal injection) was utilized to euthanatize the animal before repeating outflow measurements in deceased animals (Fig. 1B).

### 2.2. Circumlimbal suture implantation and removal

The circumlimbal suture model to induce ocular hypertension (OHT) in mice has been described previously (He et al., 2018; Zhao et al., 2017). In brief, a 10/0 nylon micro-surgical suture with attached needle was weaved over and under the conjunctiva 1 mm posterior to the limbus. The suture was threaded about 4–5 times (anchor points) underneath the conjunctiva to secure the suture in place for each eye. Care was taken to avoid penetrating the sclera. A slip-knot was made which facilitated adjustment of the inward force of compression, after weaving the suture around the eyeball. Once the target IOP (~30–40 mmHg) was reached, a second normal knot was tied to maintain the tension (He et al., 2018). The knot was made in the superior quadrant (around 12 o'clock) of the eyeball, and the end of the suture was trimmed to less than a 1 mm. In most of the animals in the OHT group, the knot and the tip of suture were embedded into the conjunctiva 1 week after the surgery. The knot was checked daily and if found to protrude it was trimmed using fine ophthalmological scissors to minimise any discomfort. Throughout the procedure corneal dehydration was avoided using a thick ophthalmic lubricating eye gel (GenTeal, 0.3% hypromellose, 0.22% carbomer 980; Novartis Pharmaceuticals, Macquarie Park, NSW, Australia). In the sham group, circumlimbal suture implantation was also performed. Two days later, under isoflurane anesthesia, the suture was cut and carefully removed to normalize IOP. This sham group comprised the sham control, where an initial IOP spike was induced and surgical procedure was replicated but no chronic IOP elevation ensued (Fig. 3B and C).

### 2.3. IOP measurement

IOP was measured in both conscious and anesthetized animals, without topical anesthesia, utilizing a handheld rebound tonometer (TonoLab, Icare Finland Oy, Vantaa, Finland). To achieve reliable measurements, 10 repeated single readings were recorded for each eye.

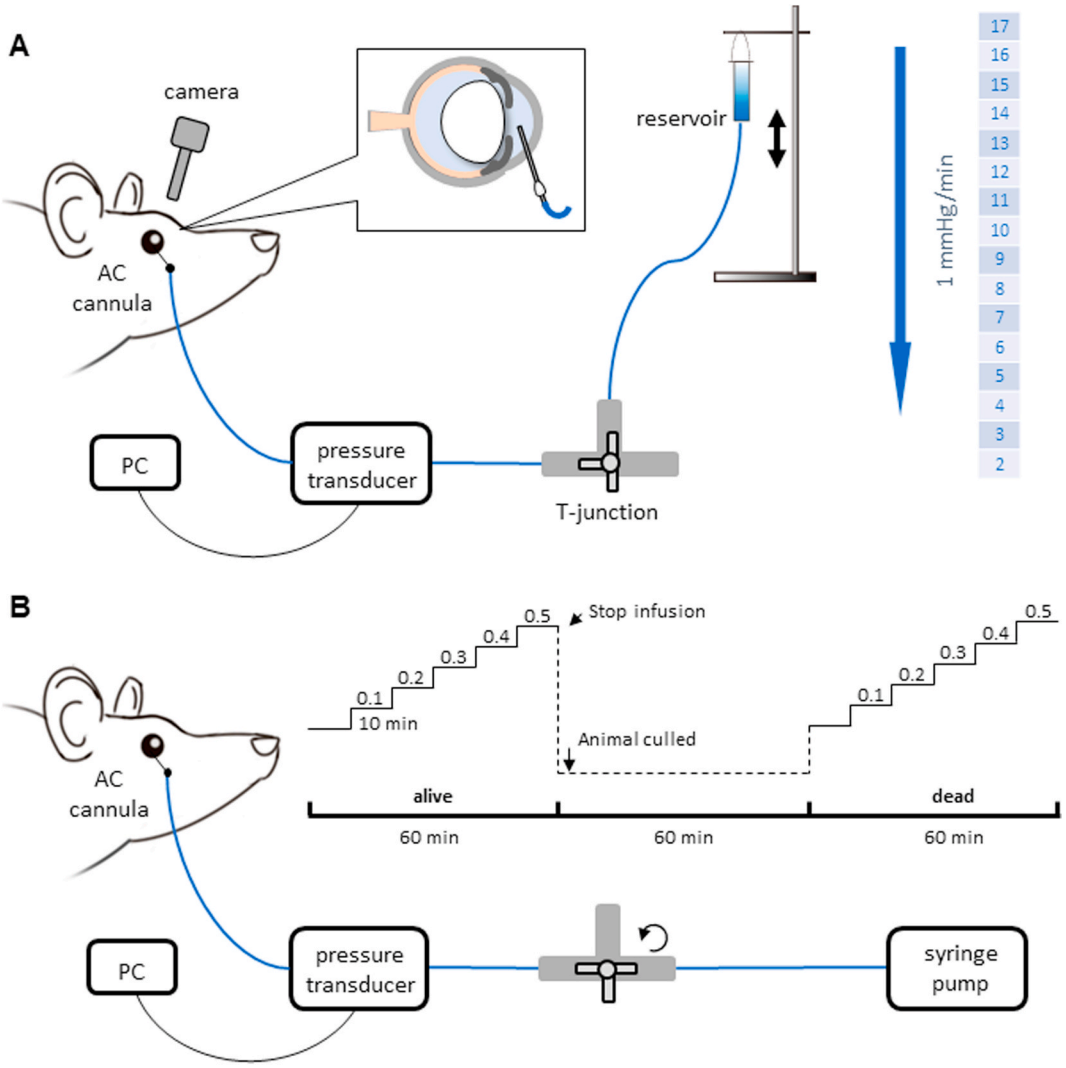


**Fig. 1.** Schematic diagram of constant-flow infusion model in mice. (A) The anterior chamber was cannulated with a 30G needle and connected via polyethylene tubing to a pressure transducer and via a 3-way T junction to a fluid filled reservoir. To estimate EVP the height of the saline reservoir was slowly and systematically lowered (1 mmHg each minute) whilst the superior surface of the eye (and episcleral vessel dilation) was visualised through a surgical microscope. (B) Following EVP estimation, the constant-flow infusion method developed by Millar et al. (2011) was then employed. Briefly, fluid was delivered to the anterior chamber through a syringe pump. Pressure in response to infusion (0.1, 0.2, 0.3, 0.4, 0.5 μl/min) was monitored via the pressure transducer connected to Labchart software (acquired using a personal computer, PC). Once pressure plateaued to a particular infusion rate which took ~ 10 min the next infusion pressure was delivered. Following the maximum infusion rate of 0.5 μl/min, infusion was stopped, and the animal was culled. The same constant infusion method was then applied (0.1, 0.2, 0.3, 0.4, 0.5 μl/min) and from these the parameters *C, Fu, Fin* could be derived.

A detailed time-course of IOP elevation following suture implantation has previously been reported from our group in mice (Zhao et al., 2017, 2019) and rats (Liu et al., 2015). These studies indicate that the highest IOP spike occurs at ~1 h post-surgery which then settles to a chronic steady IOP elevation between 2 and 12 weeks post-suture implantation. As such in the current study IOP was measured at the key timepoints of baseline (day −1, −2, −3 prior to suture implantation), 1 h post-suture implantation (IOP peak) and at the chronic end-point measurement directly before AH dynamic measurements (6–10 weeks post-surgery, average 8 weeks).

### 2.4. Anterior segment assessment

Potential changes in anterior segments induced by the circumlimbal suture were assessed using Bioptigen optical coherence tomography (Envisu R2200 VHR, Bioptigen Inc, Wetzlar, Germany) prior to AH dynamics assessment. A telecentric lens designed for small rodent eyes (18 mm, Bioptigen) was utilized to capture images of the gross structure of the anterior segment. The mouse was placed in a 3-way adjustable stage that allowed alignment of the central apex of the cornea with the objective lens. Anterior segment images were acquired by a 4 × 4 mm volume scan (100 evenly spaced horizontal B-scans, 1000 A-scan/B-scan). An extra *en face* image of the ocular surface of each eye was also obtained for pupil size measurement. All images were processed and analysed using an open source imaging analysis software (FIJI, https://fiji.sc). Images were converted to their original size (1 pixel: 1 μm) in advance. One B-scan image through the corneal apex of each eye was used to measure the anterior chamber depth, and the iridocorneal angle. In a masked fashion, the anterior chamber depth was measured vertically from the inner surface of the cornea to the anterior surface of the lens. The iridocorneal angle was calculated as the average of both the temporal and nasal angles. Pupil size was quantified by the average of both horizontal (180°) and vertical (90°) widths from the *en face* image.

### 2.5. Constant-flow infusion model for aqueous humor dynamics assessment

To quantify AH dynamic parameters, a constant-flow infusion model in mice developed by Millar and colleagues was adapted for use in this study (Millar et al., 2011). This method returns an estimate of episcleral venous pressure (*EVP*), total outflow facility (*C*), uveoscleral outflow rate (*Fu*) and AH production rate (*Fin*). In brief, the anterior chamber was cannulated parallel to the iris with a 30G needle up to the bevel. This was connected via polyethylene tubing (0.40 × 0.80 mm, Micro-tube Extrusions, North Rocks, NSW, Australia) to a pressure transducer (Transpac, Abbott Critical Care Systems) which was connected to a pre-calibrated reservoir filled with Hanks Salt Balanced Solution (Cat# H6648, Sigma Aldrich Pty Ltd., Castle Hill, NSW, Australia) and a syringe pump (Pump 11 Elite Infuse/Withdraw Programmable Syringe Pump, Harvard Apparatus, Holliston, MA, USA) with a 5 ml luer lock syringe (Terumo Europe, Leuven, Belgium) via a 3-way stop cock (SDR Scientific, Chatswood, NSW, Australia) and larger lumen tubing. The pressure transducer was connected to an amplifier system (Bridge Amp ML110, Powerlab Amplifier ML 785, LabChart software, ADInstruments Pty Ltd, Bella Vista, NSW, Australia). By opening the system to the reservoir, and artificially lowering intracameral pressure at the rate of 1 mmHg every minute blood reflux into aqueous veins could be visualised (as described in *EVP measurement*). To determine total outflow facility, the system was opened to the syringe pump to control inflow rate (as described in *Total outflow facility measurement*) (Fig. 1).

### 2.6. EVP measurement

To obtain an estimate of episcleral venous pressure, the system was opened to the reservoir which set IOP at 17 mmHg. This reservoir was then gradually lowered (Fig. 1A) in 1 mmHg steps every minute until

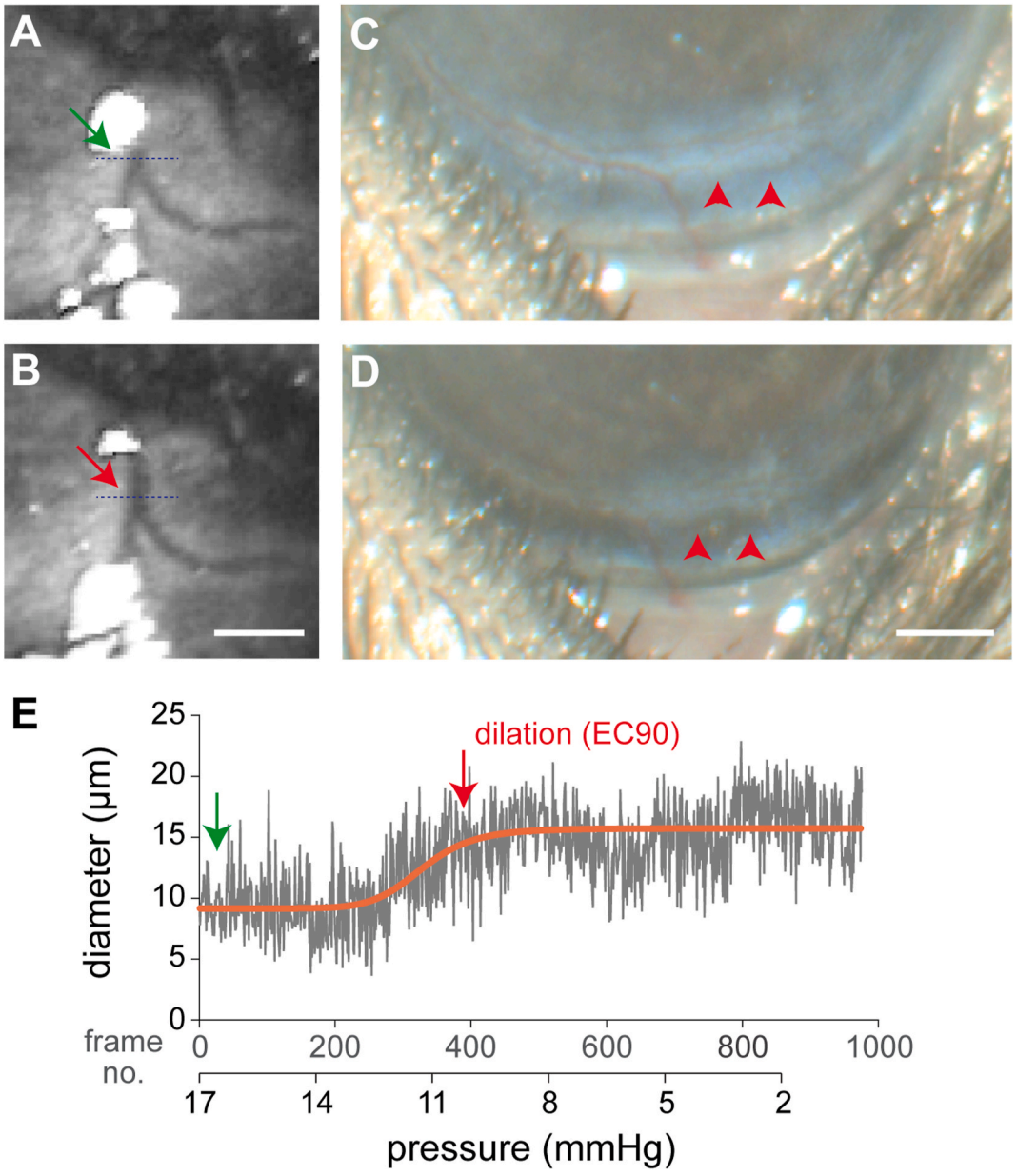


**Fig. 2.** Two methods determining episcleral venous pressure. (A, B) Representative images showing episcleral vessel dilation. Green arrow: baseline; red arrow: dilated vessel; dotted lines: ROI to measure vessel diameter. Scale bar: 50 µm. (C) Invisible Schlemm's canal at baseline (red arrowheads)and (D) blood reflux in Schlemm's canal (read arrowheads). Scale bar: 500 µm. (E) The change in vessel diameter is plotted against frame which corresponds to manometrically set eye pressure. Green arrow: baseline vessel diameter, red arrow: vessel dilation determined by EC 90 of the fitted sigmoidal function.

down to 2 mmHg. In addition to direct visualisation of blood reflux into Schlemm's canal as described by Millar et al. (2011), a camera (colour CMOS 2.3 MP, 0.5x eyepiece adaptor, XiCamTool software; Münster, Germany) was connected to a surgical microscope (STORZ Urban US-1, Tuttlingen, Germany) to record a high-resolution video (30 fps, 480p) of Schlemm's canal and one episcleral vein on the superior aspect of the eye throughout sequentially IOP (reservoir) lowering.

The exported images were analysed with FIJI software (Schindelin et al., 2012). To correct for movement during recordings images were registered using a FIJI plugin (StackReg, Translation) which minimised the mean square difference of intensities between the reference image and other images using a sub-pixel algorithm (Thevenaz et al., 1998). These videos were then viewed by a masked observer to determine the time (and associated IOP) at which blood reflux into Schlemm's canal could be observed (Fig. 2C and D). The advantage of this video approach over *in situ* assessment of blood reflux is that it can be reviewed multiple times to allow more confident and blinded assessment of EVP. In addition to visual observation of Schlemm's canal quantitative assessment of episcleral venous diameter was undertaken using the vessel diameter plugin. This was applied by placing a line of interest (LOI) perpendicular to the episcleral vein and with the vessel diameter occupying ~ 1/3 of the LOI length (Fig. 2A and B: dotted lines). The plugin quantified vessel diameter by returning the full-width at half maximum for the intensity profile of the LOI (Fischer et al., 2010). Episcleral vessel diameter was then plotted against image frame number (Fig. 2E) which was time stamped to pressure transducer measurements measured in the LabChart software (ADInstruments Pty Ltd). Changes in diameter as a function of pressure was modelled with a sigmoidal function (Equation (2)), where a F-test comparison of three models indicated this was the best fit model (Supplementary Fig. S2). The EC90 (90% efficient concentration) of this equation was then returned as an objective quantification of episcleral vessel dilation and thus measurement of EVP (Fig. 2E).

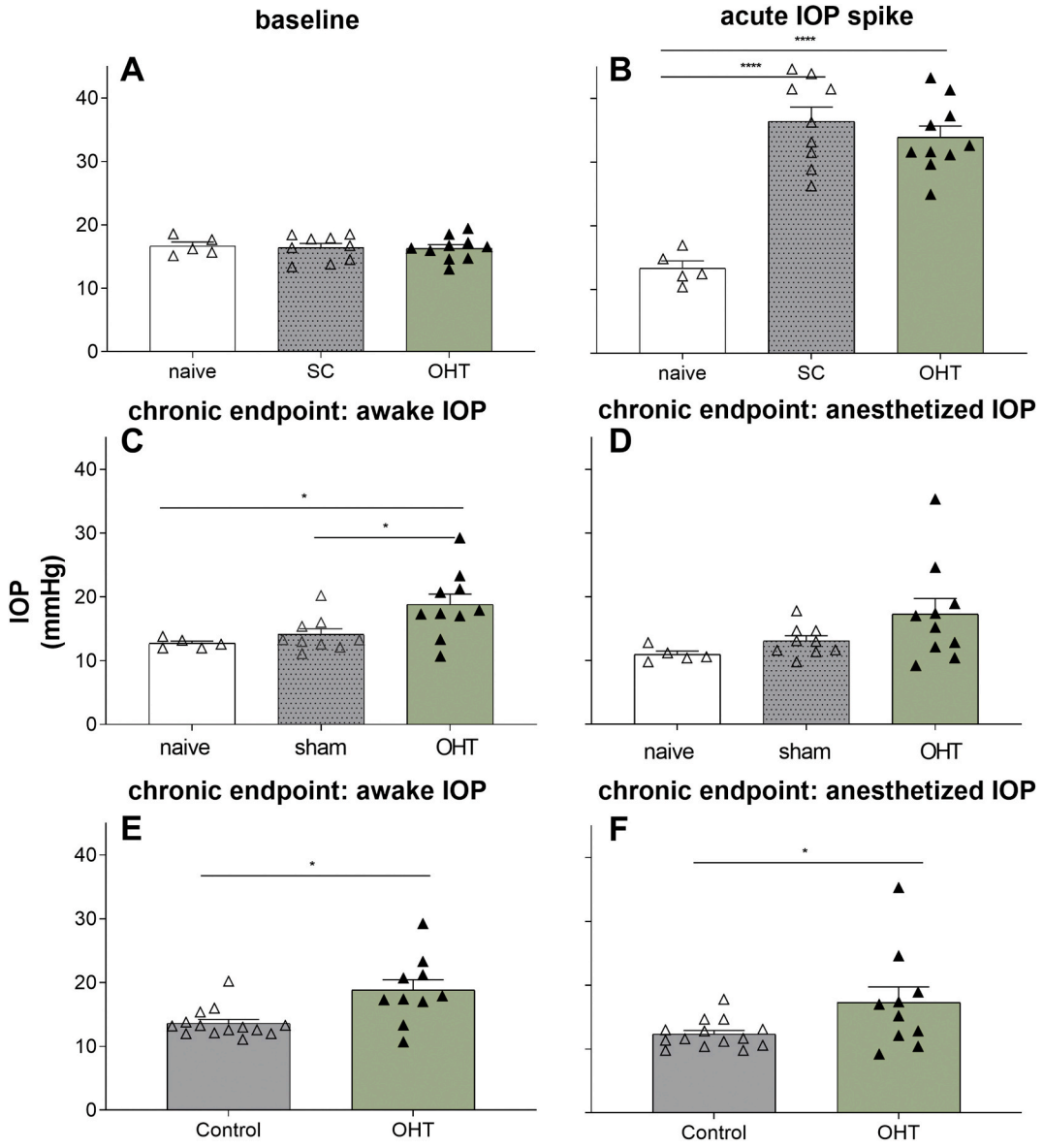


**Fig. 3.** Group average IOP in awake and anesthetized mice. (A) Baseline measurement of IOP (mmHg) in awake animals (Days −1, −2 and −3 prior to surgical procedure) and (B) at 1 h following suture implantation conducted in anesthetized mice. (C) IOP levels in the OHT group remain significantly higher at the chronic end-point in awake animals compared to naïve and sham groups, but not in anesthetized conditions, $p = 0.08$ (D). As naïve and SC groups were not significant different at end-point, IOP was combined in these groups, and (E) IOP was higher in OHT mice then control under awake and (F) anesthetized conditions. Averaged (±SEM) IOP in OHT (green), combined control (light grey), naïve (white) sham (dark grey) groups. Asterisks denotes significance: *: $p < 0.05$, ****: $p < 0.0001$.

$$diameter = \min + \left[\frac{pressure^n \cdot (max - \min)}{(pressure^n + EC50^n)}\right] \quad [2]$$

### 2.7. Total outflow facility measurement

Following return of IOP to baseline anesthetized levels via the reservoir for a minimum of 10 min the system was opened to the syringe pump via the 3-way T-junction to determine total outflow facility (Fig. 1B). The infusion rate of the pump started at 0.1 μL/min and was gradually increased to 0.5 μL/min in 0.1 μL steps. The transition between each infusion rate was initiated after IOP had plateaued as monitored using LabChart software. Typically, it took 10 min or more for IOP to plateau to each infusion rate. The IOP level at this plateau phase was plotted against infusion rate. A linear function (y = mx + c) was fit to this data, where the inverse of the slope returned total outflow facility ($C$; μL/min/mmHg). This protocol was repeated in the same animal 60 min following euthanasia via an overdose of ketamine injection. By doing so, the outflow facility in alive and dead animals could be determined which facilitates estimation of uveoscleral outflow ($F_u$) and aqueous production ($F_{in}$) as shown by Millar et al. (2011).

### 2.8. Estimation of $F_u$ and $F_{in}$

In this study, the uveoscleral outflow ($F_u$) and AH production rate ($F_{in}$) is indirectly estimated by utilizing the modified Goldmann equation (Equation (1)) to estimate $F_u$ and $F_{in}$ (Millar et al., 2011). When the syringe pump was infusing, the equation could be adjusted to:

$$IOP_{pump} = \left[\frac{(F_{pump} + F_{in} - F_u)}{C}\right] + EVP \quad [3]$$

where the $IOP_{pump}$ refers to the IOP measured when the pump was on, and the $F_{pump}$ is the infusion flow rate. $F_{in}$ and $EVP$ were considered negligible in dead animals; thus Equation (2) was modified and transformed as:

$$F_u = F_{pump} - C \cdot IOP_{pump} \quad [4]$$

where the $Fu$ and $C$ indicate uveoscleral outflow and calculated total outflow facility, respectively. $C$ is assumed as same as $C$ in dead animals ($C = C_{dead}$, tested in *Results*). $Fu$ was calculated by the average of five values generated from the five flow rates ($F_{pump}$).

Finally, the last undetermined parameter $F_{in}$ in Equation (1) can be estimated by transforming Equation (4) as follows:

$$F_{in} = [(IOP - EVP)C] + F_u \quad [5]$$

where $F_u$ is uveoscleral outflow calculated by Equation (3), and $C$ is measured in alive mice. Therefore, all the other parameters were submitted into Equation (4) to calculate $F_{in}$.

### 2.9. Statistical analysis

Group data are represented as mean ± SEM with individual data points overlaid, and significance was established with $\alpha = 0.05$. Outliers were excluded via two means. Firstly, if bleeding occurred during cannulation which would alter aqueous dynamics the animal was excluded. Secondly, Grubb's test was used as a statistical comparator to exclude outliers from further analysis. All data were determined to be normally distributed using a Kolmogorov-Smirnov test. Statistical comparison was carried out using one-way or two-way ANOVA to determine treatment effects, with post-hoc multiple comparison performed using Tukey's test and Dunnett's test, respectively. Unpaired t-tests was performed in the sham and naïve groups. Data were displayed across the three groups (naïve, sham and OHT) for IOP measurements as the initial acute IOP spike is different between naïve and sham groups. For all other measures no statistical differences were found between sham and naïve groups (Supplementary Table 1). As such data for these two groups were combined and considered to be the combined "control group".

## 3. Results

### 3.1. IOP elevation on sutured eyes

Fig. 3 shows the IOP measured in awake and anesthetized mice in naïve, sham and OHT groups. In Fig. 3A–D groups are illustrated separately, in Fig. 3E and F naïve and sham groups are combined given at the chronic end-point no statistical differences were found between these groups. IOP levels were similar between all groups at baseline (Fig. 3A). An IOP spike after circumlimbal suture implantation was evident in both sham and OHT groups (Fig. 3B sham: 40.2 ± 2.1 mmHg, n = 9, vs. OHT: 38.2 ± 2.5 mmHg, n = 10, p = 0.55; at 1 h after suturing). After suture removal (day 2), IOP in the sham group declined to levels similar to the naïve group and remained so until the end point (Fig. 3C and E). IOP in the OHT group remained higher than sham and naïve eyes throughout the experimental period. As shown in Fig. 3E, in conscious animals IOP was significantly increased in the OHT group (18.8 ± 1.6 mmHg, n = 10, $p < 0.01$) compared with the combined control group (13.6 ± 0.6 mmHg, n = 14). Similarly, Fig. 3F shows that in anesthetized mice IOP in the OHT group was higher IOP than controls (+5.2 ± 2.2 mmHg; $p < 0.05$).

### 3.2. Effects of circumlimbal suture on anterior segments

To determine whether the suture implantation induced chronic angle closure, anterior segment OCT was conducted during the chronic phase of IOP elevation. Fig. 4A and B shows representative images *en face* images of the pupil in a sutured and a control eye after 8 weeks of IOP elevation, respectively. The pupil remained circular in shape and was similar in size between the sutured and control eye (Fig. 4E, OHT: 1912 ± 101 μm, n = 9 vs. control: 1972 ± 24 μm, n = 9; p = 0.52). Fig. 4C and D shows that the anterior eye configurations were similar between control and IOP-treated eyes. Specifically, anterior chamber (AC) depth (Fig. 4F OHT: 290.8 ± 3.9 μm vs. control: 291.1 ± 3.7 μm; p = 0.93) and iridocorneal angles were similar between groups (Fig. 4G OHT: 26 ± 1° vs. control: 25 ± 2°; p = 0.98) indicating that suture implantation did not cause angle closure or narrow angles in these mice.

### 3.3. Effects of circumlimbal suture on EVP

In Fig. 5, EVP was estimated by both direct observation of blood reflux (Fig. 5A) into Schlemm's canal and by objective quantification of vessel dilation (5B). EVP was significantly higher in the OHT group (13.0 ± 1.5 mmHg) compared with the control group (7.7 ± 0.6 mmHg) when determined by blood reflux ($p < 0.01$). Similarly, when EVP was assayed by objectively quantifying of episcleral vein dilation (Fig. 5B), OHT eyes (11.7 ± 0.9 mmHg) had significantly higher EVP compared to control eyes (8.0 ± 0.7 mmHg, $p < 0.01$).

Episcleral venous pressure determined by blood reflux and vessel dilation (Fig. 5C) were significantly correlated ($R^2 = 0.48$, $Y = 0.91*X + 1.29$; 95%CI: slope: 0.49–1.33, Y-intercept: −2.9 - 5.5) suggesting the EVP determined by these two methods were comparable.

### 3.4. Effects of circumlimbal suture on outflow facility, $F_u$ and $F_{in}$

Fig. 6A compares the trabecular meshwork outflow facility ($C$) in control and OHT groups in both alive and dead conditions. When the mouse was alive, the outflow facility in OHT eyes (0.016 ± 0.002 μL/min/mmHg) was very to control eyes (0.014 ± 0.002 μL/min/mmHg). When the outflow facility measurement was repeated in dead animals, there was still no difference between the control and OHT groups (control: 0.017 ± 0.003 μL/min/mmHg vs. OHT: 0.021 ± 0.003 μL/min/mmHg). Two-way ANOVA analysis suggests that outflow facility

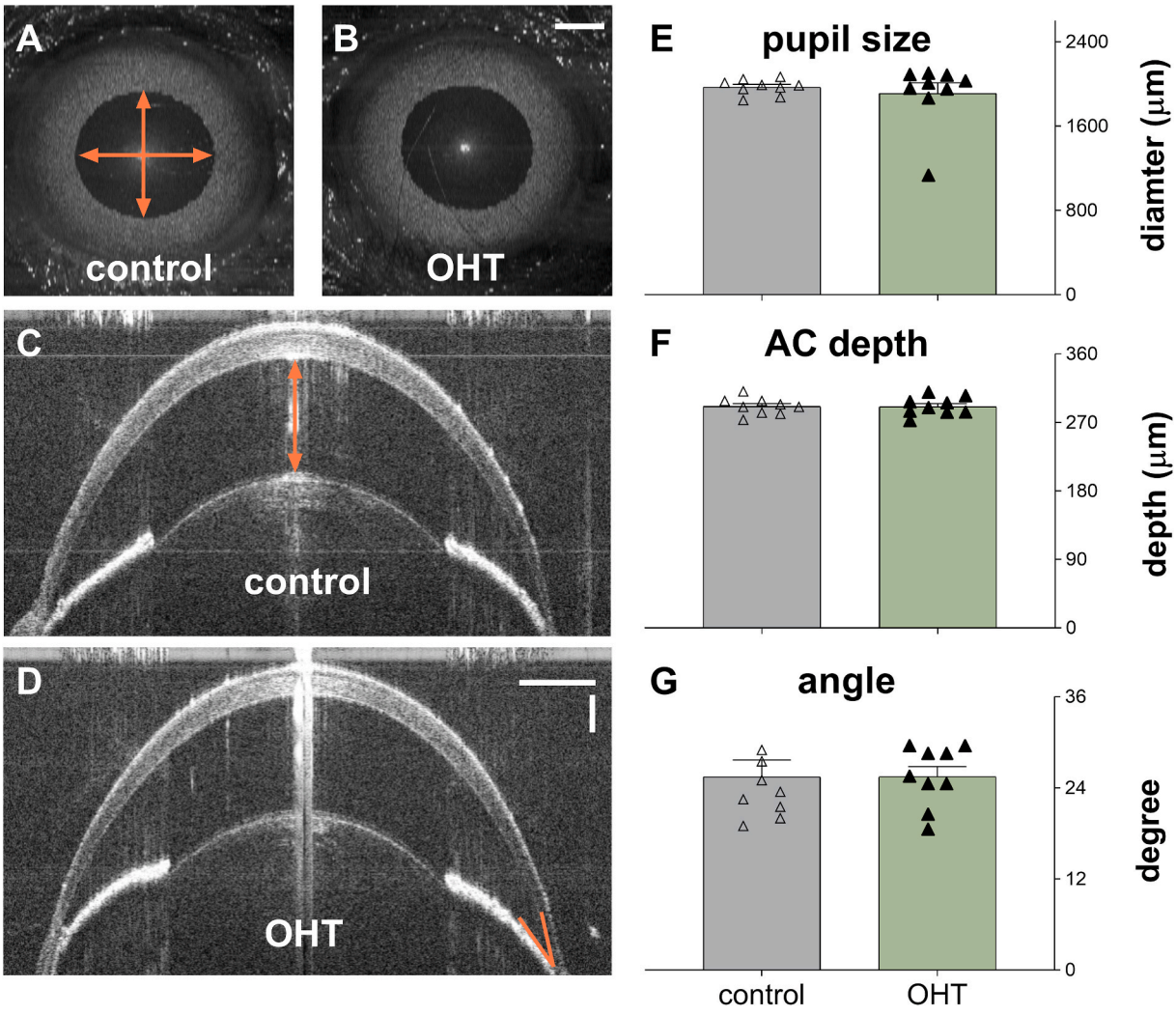


**Fig. 4.** Comparison of anterior segments between OHT and control eyes. (A-B) Representative images showing similar pupil size between control and OHT eyes. Scale bar: 1 mm. (C) Anterior chamber OCT images in a control eye and (D) IOP-treated eye. Scale bars, vertical: 100 μm, horizontal: 500 μm. Averaged group data of (E) pupil size, (F) anterior chamber depth and (G) iridocorneal angle in OHT and control groups. OHT: ocular hypertension, OCT: optical coherence tomography, AC: anterior chamber.

remained unchanged in OHT eyes ($p > 0.05$), and also there was no difference between alive and dead mice in this model ($p > 0.05$). Therefore, outflow facility in dead animals was utilized as a substitution of $C$ in alive animals to calculate uveoscleral venous flow as per Millar et al. (2011).

Fig. 6B shows the uveoscleral venous flow ($F_u$) calculated when the animal was dead according to Equation (3). It is interesting to note that there was a trend for $F_u$ to be smaller in the control group (0.01 ± 0.07 μL/min), however this was not statistically different to OHT eyes (0.14 ± 0.05 μL/min, $p = 0.17$). Aqueous humor generation rate ($F_{in}$) can be calculated according to Equation (5) by substituting all other measured and calculated parameters (Fig. 6C). There was no statistical difference between OHT eyes and control eyes (0.21 ± 0.06 μL/min vs. 0.07 ± 0.07 μL/min, $p = 0.17$). This indicates that outflow facility, uveoscleral outflow and AH production were not affected by the circumlimbal suture. Correlation between EVP and IOP.

Awake IOP and EVP for individual eyes is plotted in Fig. 7. Linear regression analysis returns a strong a correlation between IOP and EVP ($R^2 = 0.35$; $Y = 0.47*X + 2.61$; non-zero slope: $p < 0.01$). This suggests IOP elevation linearly correlated to increased EVP.

## 4. Discussion

### 4.1. Episcleral vein dilation is an objective method to estimate EVP

We used two methods to estimate EVP in this study. Currently, direct observation of blood reflux into Schlemm's canal during gradual intracameral pressure lowering is the most well-established method to estimate EVP in murine models (Aihara et al., 2003b; Millar et al., 2011; Sit and McLaren, 2011). In a normal eye, aqueous humor is constantly generated by the ciliary body and drained into Schlemm's canal which feeds into the episcleral venous network. This outflow is driven by the pressure difference between the intracameral pressure (higher) and EVP. When the EVP is marginally greater than intracameral pressure, blood from the episcleral veins will flow back into Schlemm's canal, and this blood reflux can be visualised through the thin sclera at the limbal region (Fig. 2D). As IOP is lowered below EVP, an increase in blood reflux will be seen until it fills Schlemm's canal. In contrast, when IOP is higher than EVP it is very difficult to visualise Schlemm's canal given that aqueous humor is clear (Fig. 2C). By determining the IOP at which Schlemm's canal becomes visible it is possible to estimate episcleral vein (EVP). This method is simple to perform but has its limitations. The time or IOP at which blood refluxes into Schlemm's canal when determined by subjective observation depends on observer reliability and sensitivity

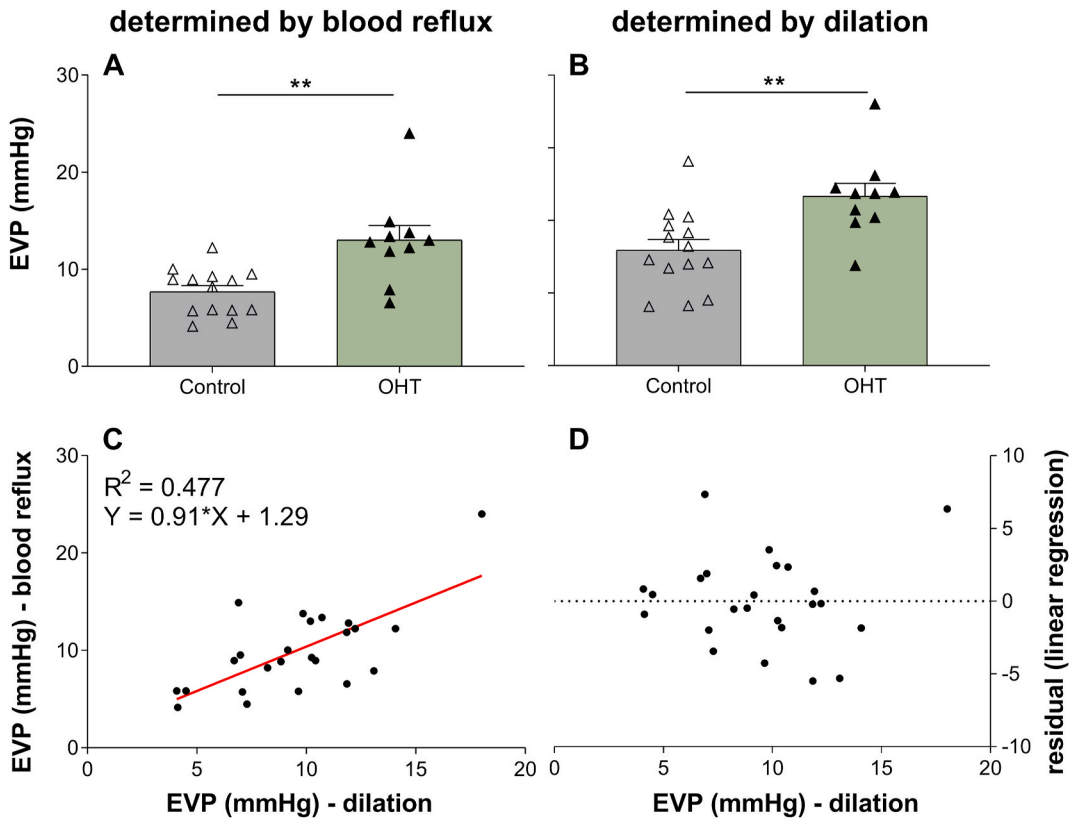


**Fig. 5.** Effects of circumlimbal suture on episcleral venous pressure. (A) EVP determined by observation of blood reflux in Schlemm's canal. EVP in OHT eyes is significantly higher than control eyes. (B) EVP significantly increased in OHT eyes than control via episcleral vessel dilation assessment. (C) Linear correlation between the two methods, where (D) shows the residual plot of the linear regression fit. Asterisks denotes significance: **: $p < 0.01$.

and can thus be highly variable. Also, a clear view of Schlemm's canal can sometimes be obstructed if the animal is heavily pigmented or has a relatively denser episcleral vasculature (Supplementary Fig. S1).

When EVP is just marginally greater than intracameral pressure, blood reflux increases the pressure inside Schlemm's canal with an associated increase in episcleral vein diameters, likely as a response to increased back pressure into these vessels. In this study, we used an automated blood vessel diameter algorithm in FIJI (Schindelin et al., 2012) to quantify episcleral vein diameter throughout IOP lowering. This diameter-pressure profile was modelled with a sigmoidal function, and the EC90 was chosen as the cut off point for vessel dilation. Comparison between this automated method and direct observation of blood reflux (Fig. 5) showed that they were significantly correlated ($R^2 = 0.48$; $Y = 0.91*X + 1.29$; $p < 0.001$), suggesting episcleral vein dilation is a reliable surrogate for EVP. Sit et al. (2011) report another approach to directly measure pressure in the episcleral veins to estimate EVP. In contrast to lowering the intracameral pressure, they delivered gradually increasing force on a small region via a venomanometer, and a high-resolution camera was simultaneously used to record the episcleral vessel. EVP was considered equal to the pressure causing episcleral vein collapse. They found that the response of the episcleral vein to pressure change was a sensitive measure, in concordance with the findings of this current study. As episcleral veins are more readily visualised above the sclera, quantifying their dilation in response to IOP lowering may be a useful objective measure of EVP in mouse eyes.

### 4.2. Elevation of episcleral venous pressure in OHT eyes

The lack of statistical difference between the sham and naïve groups indicate that the surgical procedure itself and short term IOP spike did not cause any long term alterations to aqueous dynamics. The key finding of this study was that EVP in the OHT group was significantly higher than the control group (+3.7 ± 1.2 mmHg, Fig. 5), whilst other parameters of aqueous humor dynamics remained unchanged. According to the Goldmann equation (Becker and Neufeld, 2002), IOP would be higher with EVP elevation without any other change to aqueous humor dynamics. Reduction of the pressure gradient (because of EVP elevation, Fig. 5) between the episcleral venous network and Schlemm's canal would impede aqueous fluid drainage, resulting in IOP elevation (Fig. 3). It has also been shown that IOP rapidly responds to EVP elevation, usually within 1 min (Friberg et al., 1987). It is notable that IOP elevation can still be achieved in the larger rat eye, despite efforts to thread the suture under the major episcleral veins to avoid direct compression (He et al., 2018; Liu et al., 2015). This might suggest that elevated EVP can arise from altered backflow pressure at the episcleral veins or at adjoining vasculature beds.

Our anterior segment assessment showed that the chronic suture implantation did not cause angle closure, which suggests the IOP elevation was not due to pupillary block or angle crowding mechanisms (Fig. 4). Therefore, we conjecture that the circumlimbal suture compressed the episcleral vascular network, increasing EVP, which led to impeded aqueous humor outflow and ocular hypertension. Elevated EVP has been shown to be a mechanism involved in primary open-angle glaucoma (POAG) and normal tension glaucoma (NTG) patients (Greenfield, 2000; Greslechner and Oberacher-Velten, 2019; Jorgensen and Guthoff, 1988; Selbach et al., 2005). Selbach et al. (2005) directly measured IOP and EVP in glaucoma patients and normal controls, and they showed significantly higher EVP in POAG patients (12.1 ± 0.5 mmHg, n = 32) and NTG patients (11.6 ± 0.4 mmHg, n = 36), compared to normal controls (9.5 ± 0.2 mmHg, n = 56). Consistent with our results (Fig. 7), they also demonstrated a linear relationship between IOP and EVP in glaucoma patients ($R^2 = 0.47$; $Y = 0.55*X + 9.93$). In animal studies, other rodent glaucoma models such as episcleral vein cauterization model (Ruiz-Ederra and Verkman, 2006; Shareef et al., 1995)

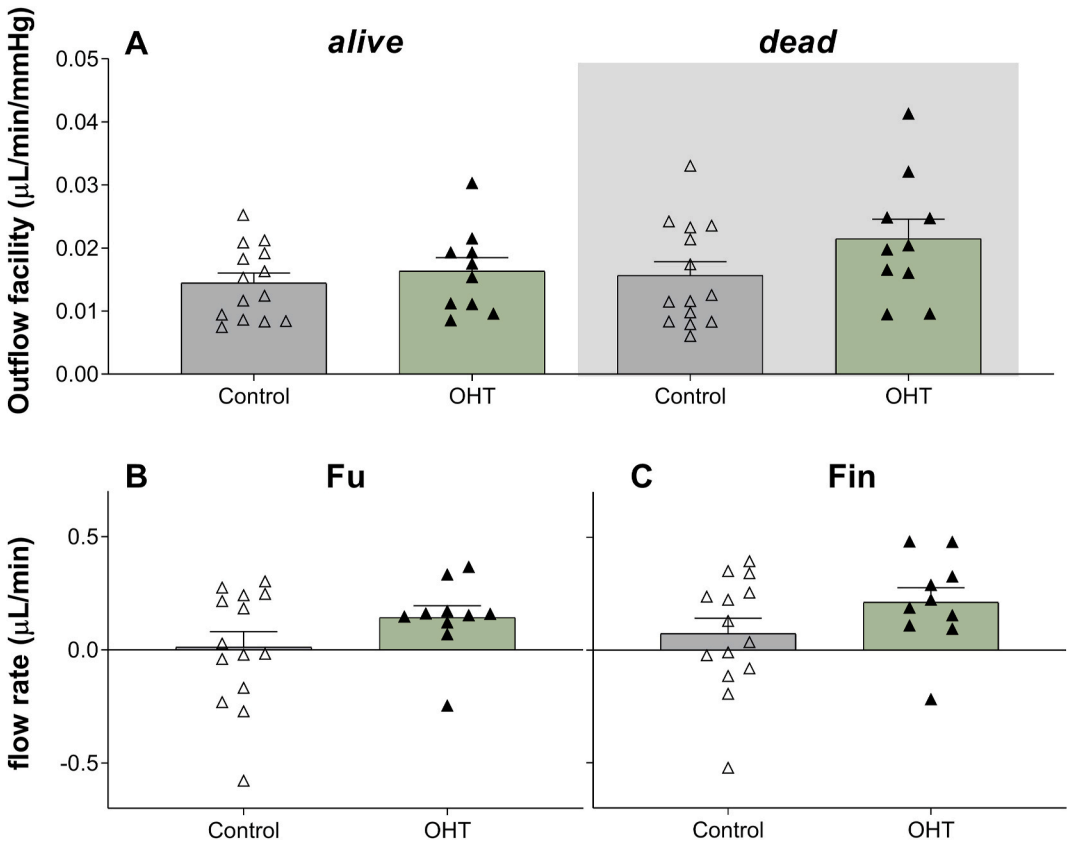


**Fig. 6.** Effect of circumlimbal suture on aqueous humor outflow facility, uveoscleral outflow and aqueous humor generation rate. (A) Aqueous humor outflow facility measured in alive and dead animals. Two-way ANOVA, $p > 0.05$. (B) Calculated uveoscleral outflow. No difference between control eyes and OHT eyes ($p = 0.17$). (C) Calculated aqueous humor generation rate. No difference between control eyes and OHT eyes ($p = 0.17$).

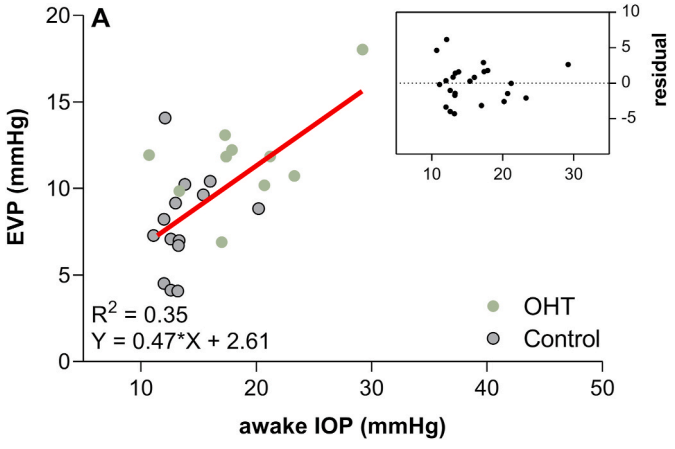


**Fig. 7.** Correlation of awake IOP at end-point and EVP in all animals. (A) Positive linear relationship was found between IOP and EVP, with a non-zero function: $Y = 0.47*X + 2.61$, $R^2 = 0.35$. *Inset:* Residual plot for the linear regression modelling the EVP vs IOP dataset.

and episcleral vein ligation model (Dey et al., 2018; Yu et al., 2006), are designed to also target elevation of EVP to induce an IOP increase. Rather than compressing the episcleral vascular network, EVP elevation in those models are achieved by obstruction of blood flow (cauterization or ligation) in a few of the main episcleral venous branches, and the reported IOP (~19 mmHg–21 mmHg in treated eyes) was similar to the circumlimbal suture model (Huang et al., 2018; Sawada and Neufeld, 1999; Zhu et al., 2012).

### 4.3. *Outflow facility and uveoscleral outflow remained unchanged in this model*

It is widely accepted that reduced outflow facility is associated with POAG (Allingham et al., 1996; Alvarado and Murphy, 1992; Becker and Hahn, 1964; Tamm and Fuchshofer, 2007). Decreased outflow facility (more resistance) effects the efficiency of aqueous humor drainage principally through the conventional pathway. Structural changes in both the trabecular meshwork and/or Schlemm's canal have been implicated in glaucoma (Grant, 1963; Johnson et al., 1992; Stamer and Acott, 2012). Some studies also show that outflow facility can be temporarily increased to compensate IOP elevation via autoregulation, which is to modify juxtacanalicular tissue structure (Bradley et al., 2001; Keller et al., 2009; Lu et al., 2008; Maepea and Bill, 1992). Our data show that IOP elevation with the circumlimbal suture was not due a reduction in total outflow facility (Fig. 6).

In mice, trabecular outflow is thought to be the predominant AH outflow pathway. However, uveoscleral outflow has been shown to be as high as ~40–50% in younger animals, but does decline as animals age (Millar and Pang, 2015). Also, the uveoscleral pathway exhibits a facility of less than 10% of total facility and is thus generally assumed to be pressure-independent. The average uveoscleral outflow rate in our mice ($0.14 \pm 0.05$ μL/min) is similar to that reported in the literature from various groups employing similar and different methods (0.115–0.148 μL/min) (Aihara et al., 2003a; Crowston et al., 2004; Lindsey and Weinreb, 2002). Uveoscleral outflow was also not altered by the circumlimbal suture model (Fig. 6B). Uveoscleral outflow and aqueous production are mathematically derived from other directly assessed parameters (Equations (4) and (5)). This may lead to seemingly "negative" measurements in individual animals (Fig. 6B and C) which is a reflection of the variability of the mathematical derivation. Direct

assessment of uveoscleral outflow (Lindsey and Weinreb, 2002) and aqueous production (Aihara et al., 2003a) may provide more accurate assessment of these parameters. However, as these approaches employ florescent dextrans and can limit simultaneous assessment of other AH measures they were not employed in the current study but would be useful in the future.

## 5. Conclusions

This is the first study to investigate the mechanism of IOP elevation induced by circumlimbal suture in mice during the chronic phase of IOP elevation. We found that sham mice who experienced an acute IOP spike (suture removed after 2 days) without any long term IOP elevation exhibited the same aqueous dynamic profiles as naïve mice. We also showed that there were no signs of angle closure in OHT mice compared with controls. We determined that EVP was higher in the OHT group compared with controls, whereas other parameters remained unchanged. These findings suggest that compression of the episcleral vascular network by the circumlimbal suture may elevated EVP which in turn results in elevated IOP.

## Supported by

Australian Research Council Linkage Grant LP160100126 (C. T. Nguyen, B. V. Bui), Melbourne Research Fellowships (C.T. Nguyen).

## Declaration of competing interest

The authors declare they have no competing interests.

## Appendix A. Supplementary data

Supplementary data to this article can be found online at https://doi.org/10.1016/j.exer.2020.108348.

## References

Aihara, M., Lindsey, J.D., Weinreb, R.N., 2003a. Aqueous humor dynamics in mice. Invest. Ophthalmol. Vis. Sci. 44, 5168–5173.
Aihara, M., Lindsey, J.D., Weinreb, R.N., 2003b. Episcleral venous pressure of mouse eye and effect of body position. Curr. Eye Res. 27, 355–362.
Allingham, R.R., de Kater, A.W., Ethier, C.R., 1996. Schlemm's canal and primary open angle glaucoma: correlation between Schlemm's canal dimensions and outflow facility. Exp. Eye Res. 62, 101–109.
Alvarado, J.A., Murphy, C.G., 1992. Outflow obstruction in pigmentary and primary open angle glaucoma. Arch. Ophthalmol. 110, 1769–1778.
Anders, F., Teister, J., Liu, A., Funke, S., Grus, F.H., Thanos, S., von Pein, H.D., Pfeiffer, N., Prokosch, V., 2017. Intravitreal injection of beta-crystallin B2 improves retinal ganglion cell survival in an experimental animal model of glaucoma. PloS One 12, e0175451.
Becker, B., Hahn, K.A., 1964. Topical corticosteroids and heredity in primary open-angle glaucoma. Am. J. Ophthalmol. 57, 543–551.
Becker, B., Neufeld, A.H., 2002. Pressure dependence of uveoscleral outflow. J. Glaucoma 11, 545.
Bradley, J.M., Kelley, M.J., Zhu, X., Anderssohn, A.M., Alexander, J.P., Acott, T.S., 2001. Effects of mechanical stretching on trabecular matrix metalloproteinases. Invest. Ophthalmol. Vis. Sci. 42, 1505–1513.
Brubaker, R.F., 2004. Goldmann's equation and clinical measures of aqueous dynamics. Exp. Eye Res. 78, 633–637.
Chen, H., Wei, X., Cho, K.S., Chen, G., Sappington, R., Calkins, D.J., Chen, D.F., 2011. Optic neuropathy due to microbead-induced elevated intraocular pressure in the mouse. Invest. Ophthalmol. Vis. Sci. 52, 36–44.
Cook, C., Foster, P., 2012. Epidemiology of glaucoma: what's new? Canadian journal of ophthalmology. J. Can. Ophtalmol. 47, 223–226.
Crowston, J.G., Aihara, M., Lindsey, J.D., Weinreb, R.N., 2004. Effect of latanoprost on outflow facility in the mouse. Invest. Ophthalmol. Vis. Sci. 45, 2240–2245.
Dey, A., Manthey, A.L., Chiu, K., Do, C.W., 2018. Methods to induce chronic ocular hypertension: reliable rodent models as a platform for cell transplantation and other therapies. Cell Transplant. 27, 213–229.
Fischer, M.D., Huber, G., Beck, S.C., Tanimoto, N., Muehlfriedel, R., Fahl, E., Grimm, C., Wenzel, A., Remé, C.E., van de Pavert, S.A., 2009. Noninvasive, in vivo assessment of mouse retinal structure using optical coherence tomography. PloS One 4, e7507.
Fischer, M.J., Uchida, S., Messlinger, K., 2010. Measurement of meningeal blood vessel diameter in vivo with a plug-in for ImageJ. Microvasc. Res. 80, 258–266.
Fortune, B., Bui, B.V., Morrison, J.C., Johnson, E.C., Dong, J., Cepurna, W.O., Jia, L., Barber, S., Cioffi, G.A., 2004. Selective ganglion cell functional loss in rats with experimental glaucoma. Invest. Ophthalmol. Vis. Sci. 45, 1854–1862.
Friberg, T.R., Sanborn, G., Weinreb, R.N., 1987. Intraocular and episcleral venous pressure increase during inverted posture. Am. J. Ophthalmol. 103, 523–526.
Goldmann, H., 1951. [Out-flow pressure, minute volume and resistance of the anterior chamber flow in man]. Documenta ophthalmologica. Adv. Ophthalmol. 5–6, 278–356.
Gong, H., Tripathi, R.C., Tripathi, B.J., 1996. Morphology of the aqueous outflow pathway. Microsc. Res. Tech. 33, 336–367.
Grant, W.M., 1963. Experimental aqueous perfusion in enucleated human eyes. Arch. Ophthalmol. 69, 783–801.
Greenfield, D.S., 2000. Glaucoma associated with elevated episcleral venous pressure. J. Glaucoma 9, 190–194.
Greslechner, R., Oberacher-Velten, I., 2019. [Glaucoma due to elevated episcleral venous pressure. Ophthalmologe 116 (5), 423–429.
He, Z., Zhao, D., van Koeverden, A.K., Nguyen, C.T., Lim, J.K.H., Wong, V.H.Y., Vingrys, A.J., Bui, B.V., 2018. A model of glaucoma induced by circumlimbal suture in rats and mice. JoVE 140, 58287.
Huang, W., Hu, F., Wang, M., Gao, F., Xu, P., Xing, C., Sun, X., Zhang, S., Wu, J., 2018. Comparative analysis of retinal ganglion cell damage in three glaucomatous rat models. Exp. Eye Res. 172, 112–122.
Jackson, T.L., Hussain, A., Hodgetts, A., Morley, A.M., Hillenkamp, J., Sullivan, P.M., Marshall, J., 2006. Human scleral hydraulic conductivity: age-related changes, topographical variation, and potential scleral outflow facility. Invest. Ophthalmol. Vis. Sci. 47, 4942–4946.
Jeon, C.J., Strettoi, E., Masland, R.H., 1998. The major cell populations of the mouse retina. J. Neurosci. : Off. J. Soc. Neurosci. 18, 8936–8946.
Johnson, M., Chan, D., Read, A.T., Christensen, C., Sit, A., Ethier, C.R., 2002. The pore density in the inner wall endothelium of Schlemm's canal of glaucomatous eyes. Invest. Ophthalmol. Vis. Sci. 43, 2950–2955.
Johnson, M., McLaren, J.W., Overby, D.R., 2017. Unconventional aqueous humor outflow: a review. Exp. Eye Res. 158, 94–111.
Johnson, M., Shapiro, A., Ethier, C.R., Kamm, R.D., 1992. Modulation of outflow resistance by the pores of the inner wall endothelium. Invest. Ophthalmol. Vis. Sci. 33, 1670–1675.
Johnson, T.V., Tomarev, S.I., 2010. Rodent models of glaucoma. Brain Res. Bull. 81, 349–358.
Jorgensen, J.S., Guthoff, R., 1988. [The role of episcleral venous pressure in the development of secondary glaucomas]. Klin Monbl Augenheilkd 193, 471–475.
Kass, M.A., Heuer, D.K., Higginbotham, E.J., Johnson, C.A., Keltner, J.L., Miller, J.P., Parrish 2nd, R.K., Wilson, M.R., Gordon, M.O., 2002. The Ocular Hypertension Treatment Study: a randomized trial determines that topical ocular hypotensive medication delays or prevents the onset of primary open-angle glaucoma. Arch. Ophthalmol. 120, 701–713 discussion 829-730.
Keller, K.E., Aga, M., Bradley, J.M., Kelley, M.J., Acott, T.S., 2009. Extracellular matrix turnover and outflow resistance. Exp. Eye Res. 88, 676–682.
Kwong, J.M., Quan, A., Kyung, H., Piri, N., Caprioli, J., 2011. Quantitative analysis of retinal ganglion cell survival with Rbpms immunolabeling in animal models of optic neuropathies. Invest. Ophthalmol. Vis. Sci. 52, 9694.
Lee, S.H., Sim, K.S., Kim, C.Y., Park, T.K., 2019. Transduction pattern of AAVs in the trabecular meshwork and anterior-segment structures in a rat model of ocular hypertension. Mol. Ther. Methods Clin. Dev. 14, 197–205.
Levkovitch-Verbin, H., Quigley, H.A., Martin, K.R., Valenta, D., Baumrind, L.A., Pease, M.E., 2002. Translimbal laser photocoagulation to the trabecular meshwork as a model of glaucoma in rats. Invest. Ophthalmol. Vis. Sci. 43, 402–410.
Lindsey, J.D., Weinreb, R.N., 2002. Identification of the mouse uveoscleral outflow pathway using fluorescent dextran. Invest. Ophthalmol. Vis. Sci. 43, 2201–2205.
Liu, H.H., Bui, B.V., Nguyen, C.T., Kezic, J.M., Vingrys, A.J., He, Z., 2015. Chronic ocular hypertension induced by circumlimbal suture in rats. Invest. Ophthalmol. Vis. Sci. 56, 2811–2820.
Liu, H.H., He, Z., Nguyen, C.T., Vingrys, A.J., Bui, B.V., 2017a. Reversal of functional loss in a rat model of chronic intraocular pressure elevation. Ophthalmic Physiol. Optic. 37, 71–81.
Liu, H.H., Zhang, L., Shi, M., Chen, L., Flanagan, J.G., 2017b. Comparison of laser and circumlimbal suture induced elevation of intraocular pressure in albino CD-1 mice. PloS One 12, e0189094.
Lu, Z., Overby, D.R., Scott, P.A., Freddo, T.F., Gong, H., 2008. The mechanism of increasing outflow facility by rho-kinase inhibition with Y-27632 in bovine eyes. Exp. Eye Res. 86, 271–281.
Maepea, O., Bill, A., 1992. Pressures in the juxtacanalicular tissue and Schlemm's canal in monkeys. Exp. Eye Res. 54, 879–883.
Martinez-Aguila, A., Fonseca, B., Perez de Lara, M.J., Pintor, J., 2016. Effect of melatonin and 5-methoxycarbonylamino-N-acetyltryptamine on the intraocular pressure of normal and glaucomatous mice. J. Pharmacol. Exp. Therapeut. 357, 293–299.
Mermoud, A., Baerveldt, G., Minckler, D.S., Prata Jr., J.A., Rao, N.A., 1996. Aqueous humor dynamics in rats. Graefes Arch. Clin. Exp. Ophthalmol. 234 (Suppl. 1), S198–S203.
Millar, J.C., Clark, A.F., Pang, I.H., 2011. Assessment of aqueous humor dynamics in the mouse by a novel method of constant-flow infusion. Invest. Ophthalmol. Vis. Sci. 52, 685–694.
Millar, Cameron J., Pang, Iok-Hou, 2015. Non-continuous measurement of intraocular pressure in laboratory animals. Exp Eye Res 141, 74–90. https://doi.org/10.1016/j.exer.2015.04.018.
Pang, I.H., Clark, A.F., 2007. Rodent models for glaucoma retinopathy and optic neuropathy. J. Glaucoma 16, 483–505.

Pollet-Villard, F., Chiquet, C., Romanet, J.P., Noel, C., Aptel, F., 2014. Structure-function relationships with spectral-domain optical coherence tomography retinal nerve fiber layer and optic nerve head measurements. Invest. Ophthalmol. Vis. Sci. 55, 2953–2962.

Ruiz-Ederra, J., Verkman, A.S., 2006. Mouse model of sustained elevation in intraocular pressure produced by episcleral vein occlusion. Exp. Eye Res. 82, 879–884.

Saleh, M., Nagaraju, M., Porciatti, V., 2007. Longitudinal evaluation of retinal ganglion cell function and IOP in the DBA/2J mouse model of glaucoma. Invest. Ophthalmol. Vis. Sci. 48, 4564–4572.

Sawada, A., Neufeld, A.H., 1999. Confirmation of the rat model of chronic, moderately elevated intraocular pressure. Exp. Eye Res. 69, 525–531.

Schindelin, J., Arganda-Carreras, I., Frise, E., Kaynig, V., Longair, M., Pietzsch, T., Preibisch, S., Rueden, C., Saalfeld, S., Schmid, B., Tinevez, J.Y., White, D.J., Hartenstein, V., Eliceiri, K., Tomancak, P., Cardona, A., 2012. Fiji: an open-source platform for biological-image analysis. Nat. Methods 9, 676–682.

Selbach, J.M., Posielek, K., Steuhl, K.P., Kremmer, S., 2005. Episcleral venous pressure in untreated primary open-angle and normal-tension glaucoma. Ophthalmologica 219, 357–361.

Shareef, S.R., Garcia-Valenzuela, E., Salierno, A., Walsh, J., Sharma, S.C., 1995. Chronic ocular hypertension following episcleral venous occlusion in rats. Exp. Eye Res. 61, 379–382.

Sit, A.J., Ekdawi, N.S., Malihi, M., McLaren, J.W., 2011. A novel method for computerized measurement of episcleral venous pressure in humans. Exp. Eye Res. 92, 537–544.

Sit, A.J., McLaren, J.W., 2011. Measurement of episcleral venous pressure. Exp. Eye Res. 93, 291–298.

Smedowski, A., Pietrucha-Dutczak, M., Kaarniranta, K., Lewin-Kowalik, J., 2014. A rat experimental model of glaucoma incorporating rapid-onset elevation of intraocular pressure. Sci. Rep. 4, 5910.

Stamer, W.D., Acott, T.S., 2012. Current understanding of conventional outflow dysfunction in glaucoma. Curr. Opin. Ophthalmol. 23, 135–143.

Tamm, E.R., 2009. The trabecular meshwork outflow pathways: structural and functional aspects. Exp. Eye Res. 88, 648–655.

Tamm, E.R., Fuchshofer, R., 2007. What increases outflow resistance in primary open-angle glaucoma? Surv. Ophthalmol. 52 (Suppl. 2), S101–S104.

Thevenaz, P., Ruttimann, U.E., Unser, M., 1998. A pyramid approach to subpixel registration based on intensity. IEEE Trans. Image Process. 7, 27–41.

Viswanathan, S., Frishman, L.J., Robson, J.G., Walters, J.W., 2001. The photopic negative response of the flash electroretinogram in primary open angle glaucoma. Invest. Ophthalmol. Vis. Sci. 42, 514–522.

Yu, S., Tanabe, T., Yoshimura, N., 2006. A rat model of glaucoma induced by episcleral vein ligation. Exp. Eye Res. 83, 758–770.

Zhan, G.L., Lee, P.Y., Ball, D.C., Mayberger, C.J., Tafoya, M.E., Camras, C.B., Toris, C.B., 2002. Time dependent effects of sympathetic denervation on aqueous humor dynamics and choroidal blood flow in rabbits. Curr. Eye Res. 25, 99–105.

Zhao, D., Nguyen, C.T., Wong, V.H., Lim, J.K., He, Z., Jobling, A.I., Fletcher, E.L., Chinnery, H.R., Vingrys, A.J., Bui, B.V., 2017. Characterization of the circumlimbal suture model of chronic IOP elevation in mice and assessment of changes in gene expression of stretch sensitive channels. Front. Neurosci. 11, 41.

Zhao, D., Wong, V.H.Y., Nguyen, C.T.O., Jobling, A.I., Fletcher, E.L., Vingrys, A.J., Bui, B. V., 2019. Reversibility of retinal ganglion cell dysfunction from chronic IOP elevation. Invest. Ophthalmol. Vis. Sci. 60, 3878–3886.

Zhu, Y., Zhang, L., Schmidt, J.F., Gidday, J.M., 2012. Glaucoma-induced degeneration of retinal ganglion cells prevented by hypoxic preconditioning: a model of glaucoma tolerance. Mol. Med. 18, 697–706.